

Neural network estimations of annealed and non-annealed Schottky diode characteristics at wide temperatures range

Hülya Doğan^{a,*}, Songül Duman^b, Yunis Torun^a, Serkan Akkoyun^c, Seydi Doğan^d, Uğur Atıcı^e

^a Department Electrical and Electronics Engineering, Faculty of Engineering, Sivas Cumhuriyet University, Sivas, Turkey

^b Department of Basic Sciences, Faculty of Science, Erzurum Technical University, 25050, Erzurum, Turkey

^c Department of Physics, Faculty of Science, Sivas Cumhuriyet University, Sivas, Turkey

^d Department of Electrical and Electronics Engineering, Faculty of Engineering, Balıkesir University, Balıkesir, Turkey

^e Department Industrial Engineering, Faculty of Engineering, Sivas Cumhuriyet University, Sivas, Turkey



ARTICLE INFO

Keywords:

Schottky diode

Artificial neural network

Modelling

ABSTRACT

In this study, Artificial Neural Network (ANN) model has been proposed to characterize the annealed and the non-annealed Schottky diode from experimental data. The experimental current values of Ni/n-type 6H-SiC Schottky diode for the voltages applied to the diode terminal starting from 80 K with 20 K steps up to 500 K temperature were measured for both non-annealed and annealed Schottky diodes. The applied voltage has been varied starting from -2 V with 10 mV steps up to +2 V for each temperature value. The modeling performance has been assessed according to the varying number of neurons in the hidden layer, starting from 5 to 50 neurons, thereafter the optimum number of neurons has been obtained for both annealed and non-annealed ANN models. The minimum Root Mean Square Error (RMSE) and Mean Absolute Error (MAE) indices values for both annealed and non-annealed diodes have been obtained with 40 neurons for both the training and test phase.

1. Introduction

Metal/semiconductor (MS) contact has an ohmic or rectifier structure [1]. The Schottky barrier diode (SBD) is called the rectifier MS contact, and as it is a majority carrier-based device, it provides a significant advantage in terms of speed. However, SBDs are widely used in radio frequency and other power electronics applications [2]. Investigation of the newly produced MS structures and their electrical properties is of critical importance in determining the usage areas of these devices [3,4]. Whether a diode has high performance is determined by parameters such as ohmic contact, stability under high temperature, and breakdown voltage [5]. Working under high thermal conditions is one of the key performance indicators for diodes. Most silicon-based conventional integrated circuit technology (IC) cannot operate at temperatures above 250 °C. The characteristic of the IC changes and cannot perform the desired task properly when high operating temperatures are combined with high-power, high-frequency and high-radiation environments [6]. Silicon Carbide (SiC) has become a vital semiconductor due to its unique electrical and optical features [7–11]. SiC-based devices have proven to be an important semiconductor candidate for commercially demanding tasks such as harsh ambient temperature sensing [12,

13]. Due to a wide bandgap has a small leakage current and small minority carrier formation rate [14,15]. It is preferred for high-temperature electronic devices since it shows its inert property at very high temperatures (over 800 °C) [16,17]. It is used in switching and high voltage applications, about ten times more than Si, due to its high-breakdown electric field. Because it has good thermal conductivity and high thermal stability, it is preferred in high-temperature applications and thermal heat dissipation. Since it is the only compound semiconductor with only natural oxide, it is possible to use it in MOSFET construction [18–21].

Due to its more isotropic effective mass than others (3H-SiC and 6H-SiC), 4H-SiC has greater electron mobility and is almost independent of crystallographic orientation [22]. In addition to having a wider band gap compared to 4H-SiC, 6H-SiC and 3C-SiC, it has n-type and p-type properties. It can be easily obtained by doping nitrogen and aluminum elements, which is a rare property compared to other wide band gap semiconductors (especially difficult to obtain p-type in ZnO and GaN) [23]. However, especially for thermal sensitivity or cryogenic temperature applications, 6H-SiC semiconductor-based devices can exhibit high linearity and sensitivity as a function of the forward constant current level. In addition, SiC-based Schottky diodes with different

* Corresponding author.

E-mail address: hdogan@cumhuriyet.edu.tr (H. Doğan).

material contacts have various low and high temperature applications as temperature sensing elements. The development of high-temperature sensors based on SiC SBDs that can operate in harsh conditions requires the use of a high-barrier Schottky contact such as Ni as the Schottky contact metal [12–14,24–26]. Roccaforte et al. [27], investigated that annealing in a vacuum environment in the temperature range of 400–650 °C causes a Ni/Ti/SiC reaction above 450 °C and observed the formation of nickel silicides such as $\text{Ni}_{31}\text{Si}_{12}$ and Ni_2Si as a result of this reaction. They also observed inhomogeneous Ni-silicide/SiC barriers at around 600 °C. From the early studies on Ni/SiC contacts, it was observed that the nickel film should be annealed at at least 900–950 °C for a good ohmic contact [28]. Below these temperatures, only a rectifying behavior was observed. The first explanation of this behavior was due to Su and Steckl [29], who reported that the interface between Ni and SiC remained the same as before annealing up to 600 °C. This means that nickel silicide is not formed and in fact the contact remains rectifying. Vasilevski et al. [30] annealed Ti/4H-SiC and Ni/4H-SiC Schottky diodes at 550 °C in vacuum. They [30] investigated the I-V characteristics of 4H-SiC Schottky diodes in the temperature range from room temperature to 400 °C and showed that the diodes Schottky barrier height and ideality factor did not change. La Via et al. [31] investigated the interfacial reaction and phase formation as a function of the annealing temperature (600 – 1000 °C) by evaporating the nickel thin film onto the n-6H-SiC (0001) substrate. They [31] observed the only nickel silicide phase (Ni_2Si) between 600 and 950 °C using a combination of Rutherford Backscattering Spectrometer, X-Ray Diffraction, Transmittance Electron Microscopy, and layer resistance measurements. As a result, they concluded from the electrical characterization that an inhomogeneous Schottky barrier height was formed.

Previous studies [27,31] have shown that Ni reacts with SiC semiconductor depending on the annealing temperature. The formation of nickel silicides (Ni_2Si and $\text{Ni}_{31}\text{Si}_{12}$) in the annealing of Ni/SiC contact up to a temperature of 600 °C and then the formation of only the Ni_2Si phase was observed when annealed at a temperature higher than 950 °C. $\text{Ni}_2\text{Si}/\text{SiC}$ Schottky diodes have been reported to have nearly ideal properties ($n = 1.07$) and a barrier height of about 1.3 eV [31]. Vasilevski et al. [30] obtained high temperature silicon carbide diodes with Ti/4H-SiC and Ni/4H-SiC epitaxial sheets and annealed the diodes at 550 °C in vacuum. They [30] stated that annealing at 550 °C leads to Ni_2Si film formation and these nickel silicide Schottky contacts reveal almost ideal electrical properties at forward and low reverse biases, as the excellent contact layer – semiconductor interface is formed by solid state chemical reaction.

Different optimization techniques are used to determine the electrical parameters of Schottky diodes. Equilibrium optimizer, artificial bee colony, advanced swarm intelligence, and artificial neural network are examples of the primary techniques used for this purpose [21,32,33]. Modeling of Schottky diode with artificial intelligence and machine learning techniques has become widespread in recent years [34–36]. The modeling of semiconductors devices with available experimental data provides us to characterize the nonlinear behavior of the device at any point at which there was no experimental data available. Traditional physics-based approaches with analytical equations characterizing Schottky diodes sometimes fail to keep up with rapid technological innovations in device processing complexity. Therefore, there is increasing interest in innovative approaches such as machine learning and artificial intelligence approach in the semiconductor community.

The artificial neural network (ANN) method has been used in many fields in engineering, including studies on Schottky diodes [34,35,37]. ANN is a mathematical tool that mimics human brain functionality [38].

The data for the ANN has been obtained from the experiments performed by us. The data set consists of 7840 samples for annealed Schottky diode and 5796 number samples of directly fabricated Schottky diode. Approximate modeling of Schottky diode was obtaining a Multi-Input Single Output (MISO) black-box model. The model inputs are temperature value and voltage, while the model output is Schottky

current. The non-linear relationship between inputs and output is obtained by learning and validating the ANN model from experimental current and voltage values of Schottky diodes at different temperatures steps. Once the training process is completed, the ANN model can estimate the value of the Schottky current for any voltage and temperature within the training universe. This study used a more comprehensive temperature range to train the models than recent works [34,35,39]. The proposed model can predict the non-linear relation of current versus voltage with a wide temperature range.

This study consist of four sections. The importance of the handled problem, the motivation behind this study, and related works are presented in the first section. The artificial neural network method and modeling environment are explained in the second section. Obtained results and findings are elucidated in the third section. The findings are clarified in the fourth section.

2. Materials and method

In this study, n-type wafers of 6H-SiC, Si-ended face purchased from CREE research, Inc. were used. The thickness of the n-type 6H-SiC wafers were 257 μm with a carrier concentration of $2 \times 10^{18} \text{ cm}^{-3}$. Before making Ohmic and Schottky contacts, the sample was cleaned in an ultrasonic bath with acetone, methanol, and deionized water, respectively. Then, the RCA cleaning method was then used to remove the thin oxide layer. Immediately after the cleaning process, high purity Nickel (Ni) metal was evaporated to the C-ended face of the SiC sample for the ohmic contact process and annealed in a nitrogen gas environment at 900 °C for 10 min. Ni metal in circular form with 1 mm diameter was re-evaporated to the Si-ended face of the SiC sample for Schottky contact making. All evaporation were carried out in a coating unit at approximately 10^{-6} Torr pressure. The I-V measurements of the as-fabricated diode and after annealing the same diode at 973 K which is needed for the formation of Ni_2Si phase [8,9] for 2 min were performed using a Keithley 487 Picoammeter/Voltage Source, at different temperatures, ranging between 80 and 500 K by means of a closed-cycle helium cryostat in dark conditions. The fabrication of the SBDs has been detailed in Ref. [10].

2.1. Artificial neural network method

A mathematical method, artificial neural network (ANN), is a robust tool for solving non-linear problems when standard techniques fail. It mimics the brain functionality and nervous systems [21]. ANN has neurons in different layers indicated as input, hidden, and output layers. Neurons in the input layer receive data of the problems and transmit the data to the hidden neurons in the hidden layer. In the fully-connected multilayer perceptron ANN model, all neurons are connected to each neuron in the next layer. The processed data exits the hidden neurons after summing and activating the data in the hidden neurons by proper sum and activation functions. The net signal is transmitted to the output neurons in the output layer. Again, the whole data entering the output neurons are also summed and activated by the chosen proper function.

In the present study, we have used tangent hyperbolic activation functions in the hidden and the output layer neurons, a sigmoid-like function used commonly in the literature. The data flow in a one-way forward direction between different layers; the ANN is called layered feed-forward ANN. The data transmissions between the neurons are connected via adjustable synaptic weights. Determination of the final values of the weights by using sample training data is a purpose of the ANN calculations. This first stage is known as the training stage of the ANN. The neuron numbers in input and output layers depend on the nature of the problem. In contrast, there is no rule for the number of hidden layers and neurons. They are determined after several trials, but one hidden layer ANN structure is sufficient for solving problems [17].

It is needed to give the minimum fundamentals necessary for understanding the study. For single hidden layer ANN structure, the

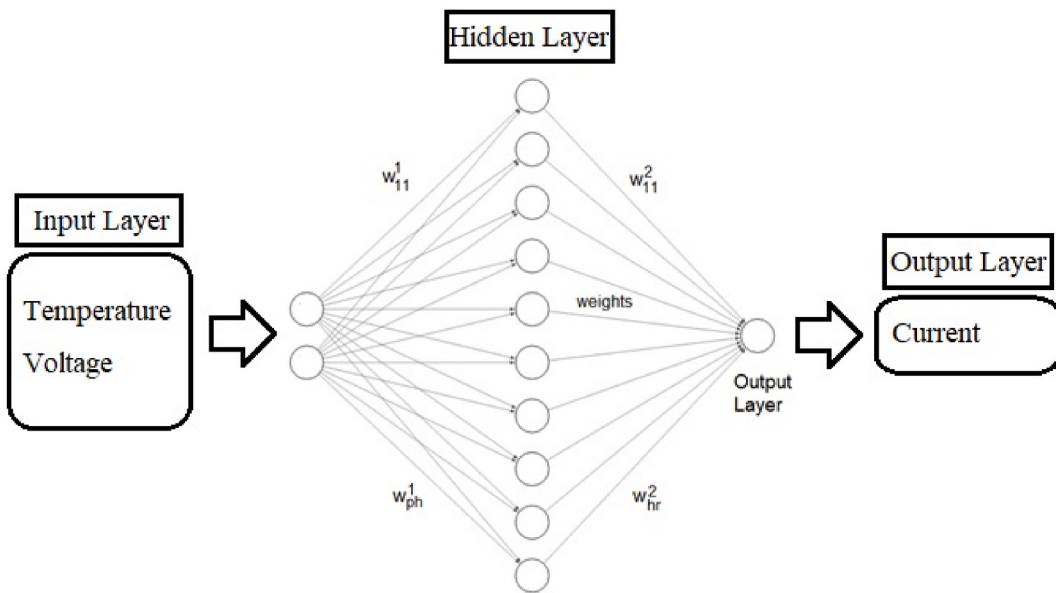


Fig. 1. One of the used ANN structure (2-10-1) for the estimation of Schottky diode characteristics under different temperature.

Table 1

RMSE and MAE values on the annealed and un-annealed training data for the ANN structures with different hidden neuron numbers.

Train Data					
Annealed			Un-annealed		
Hidden Neuron #	RMSE	MAE	Hidden Neuron #	RMSE	MAE
5	4.03E-05	1.45E-05	5	1.29E-04	3.57E-05
8	4.96E-05	1.73E-05	8	1.21E-04	3.35E-05
10	3.76E-05	1.13E-05	10	8.47E-05	2.11E-05
20	2.51E-05	9.04E-06	20	7.09E-05	1.61E-05
30	2.03E-05	7.38E-06	30	6.61E-05	1.45E-05
40	1.55E-05	4.97E-06	40	6.36E-05	1.47E-05
50	4.12E-05	1.40E-05	50	6.58E-05	1.51E-05

desired output vector \vec{y} (Current (I) in Fig. 1) is approximated by a network multi-output vector \vec{f} . The \vec{f} vector is defined by Eq. (1) as

$$\vec{f} : R^p \rightarrow R^r : \vec{f}_k(\vec{x}) = \sum_{j=1}^{h_1} \beta_j G(A_j(\vec{x})), \vec{x} \in R^p, \beta_j \in R, A_j \in A^p, \text{ and } k = 1, \dots, r \quad (1)$$

where A^p is the set of all functions $R^p \rightarrow R$ defined by $A(\vec{x}) = \vec{w} \cdot \vec{x} + b$, \vec{w} is weight vector from the input layer to hidden layer, \vec{x} is the input vector of ANN, b is the bias weight, p , and r numbers indicated the number of input and output variables, respectively. $G : R \rightarrow R$ is the activation function for the neurons? In this study, the inputs are voltage (V) and temperature (T) for the Schottky diode. We have used seven different ANN structures, and the results are comprised to see the power of the ANN with different hidden neurons with 5, 8, 10, 20, 30, 40, and 50 (see Fig. 1). The total number of adjustable weights (ΣW) in these different structures was calculated by Eq. (2) as 15, 24, 30, 60, 90, 120, and 150.

Table 2

RMSE and MAE values on the annealed and un-annealed test data for the ANN structures with different hidden neuron numbers.

Test Data					
Annealed			Un-annealed		
Hidden Neuron #	RMSE	MAE	Hidden Neuron #	RMSE	MAE
5	4.10E-05	1.43E-05	5	1.28E-04	3.40E-05
8	4.72E-05	1.67E-05	8	1.17E-04	3.20E-05
10	3.99E-05	1.14E-05	10	7.90E-05	2.04E-05
20	2.73E-05	9.47E-06	20	6.55E-05	1.59E-05
30	1.94E-05	6.90E-06	30	6.61E-05	1.45E-05
40	1.51E-05	4.93E-06	40	5.61E-05	1.30E-05
50	4.35E-05	1.41E-05	50	5.90E-05	1.42E-05

$$\Sigma W = p.h + h.r = h.(p + r) \quad (2)$$

In Fig. 1, the weight matrices w^1 and $w^2 w^1$ and w^2 correspond to weight vectors defined in $A(\vec{x})$ and $\vec{\beta}$ in Eq. (1). As seen in Fig. 1 and Eq. (1), the correspondences $w^2 \rightarrow \vec{\beta}$ are valid only for the single hidden layer ANN structure.

ANN calculations are two main stages. The first is the training stage, and the other is the test stage. The total problem data is separated into two sets for these work stages. 80% of all data is used for the training stage, and 20% is used for the test stage. The training data that includes both inputs and the outputs of the problem is given to the ANN in the training stage. By modifying the weights between the neurons, the best weight values are sought from the inputs to reach the desired outputs.

After an acceptable error level between the ANN outputs and the experimental values in the training stage is obtained, the training stage is stopped. ANN is constructed to solve the problem with the obtained final weights. For the training of the ANN, a Levenberg–Marquardt backpropagation algorithm [40,41] was used in this work. ANN performance must be seen on the test data to decide whether constructed

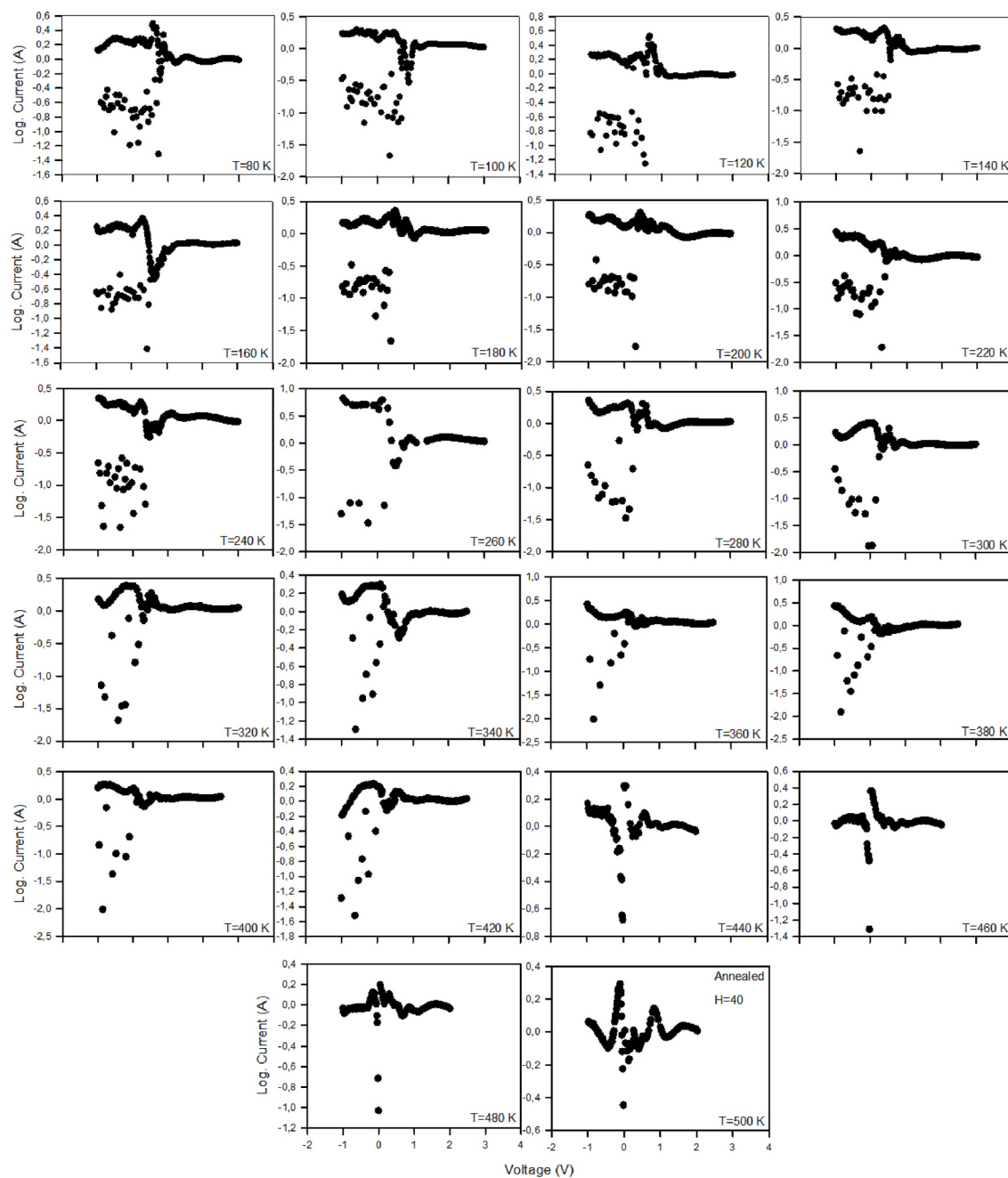


Fig. 2. Deviation between experimental and ANN estimated ($H = 40$) current values for annealed training data according to voltage values at different temperatures.

ANN is suitable for similar Schottky diode data estimations. If the ANN outputs in the test stage using final weights are still close to the desired experimental outputs, it can be concluded that the ANN is convenient for the problem's solution.

2.2. Modeling environment

The ANN models were programmed with the Neural Network Toolbox (Matlab R2018a). The model codes have been run on a desktop computer with a 4th generation i7 processor with 16 Gb RAM. The acquired experimental data has been divided into train and test phases with **5-fold cross-validation** techniques. Therefore, the data set has divided training and test data subset randomly. At the end of 5 fold, all models are trained and tested with five different training and test set combinations, so the model performance was measured by averaging

each fold. Performance assessment has been performed with calculation root mean square error (RMSE) and mean absolute error (MAE) as;

$$RMSE = \left[\frac{1}{n} \sum_{i=1}^n |I_i - \hat{I}_i|^2 \right]^{\frac{1}{2}} \quad (3)$$

$$MAE = \frac{1}{n} \sum_{i=1}^n |I_i - \hat{I}_i| \quad (4)$$

where I_i is the acquired experiment value of current (I), \hat{I}_i is the predicted current value for i th instant within the total n instant.

3. Results and discussion

We have applied seven different ANN structures to estimate the

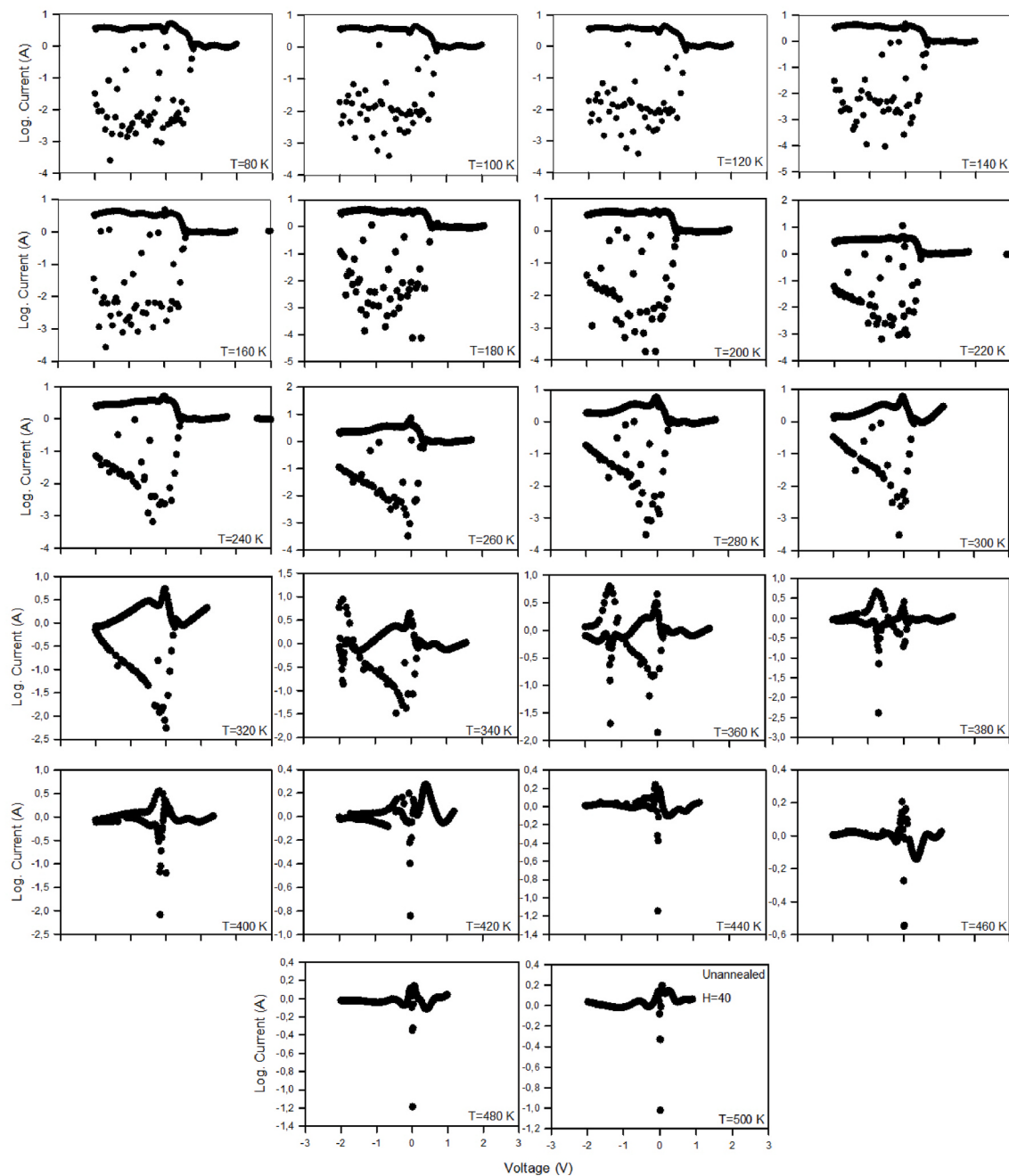


Fig. 3. Deviation between experimental and ANN estimated ($H = 40$) current values for un-annealed training data according to voltage values at different temperatures.

current values according to the voltage and temperature for Schottky diodes. We have used a logarithm of the current values to smooth the data. We had two separate experimental datasets of Schottky diodes, annealed and un-annealed. The total annealed data was partitioned into 4791 for training and 1174 for the test stage. On the other hand, we used 6274 of the un-annealed data in the training and 1567 in the test stage. The RMSE and MAE values for training data are listed in Table 1 for the different hidden neuron numbers. As can be seen from the table, the RMSE values decrease as the number of neurons used in the single hidden layer increases for the annealed data. The lowest RMSE value was reached in the ANN structure in which the number of hidden neurons was 40; then, it was observed that the RMSE value increased again as the number of neurons continued to increase. While the RMSE value is 4.03E-05 when the number of hidden layer neurons is 5, it is 1.55E-05

when it is 40. Then, in the structure where the number of hidden neurons was 50, the RMSE value increased to 4.12E-05. When the results of MAE values are examined, this value is calculated as 0.1483 when the number of hidden neurons is 30. However, the lowest value of MAE was obtained in the ANN structure, where the number of hidden neurons was 40. The highest value of MAE is in the ANN structure, where the number of hidden neurons is the lowest, that is, 8.

In the case of un-annealed data as shown in Table 2, with the increase in the number of hidden layer neurons, the RMSE value decreased to 40, then showed increases again up to 50. While the RMSE value is 1.29E-04 when the number of hidden layer neurons is 5, it is 6.36E-05 when it is 40. When the MAE values of the estimates on the un-annealed data were examined, it was seen that the lowest MAE value was obtained in the structure with 30 hidden neurons. In addition, the immense MAE value

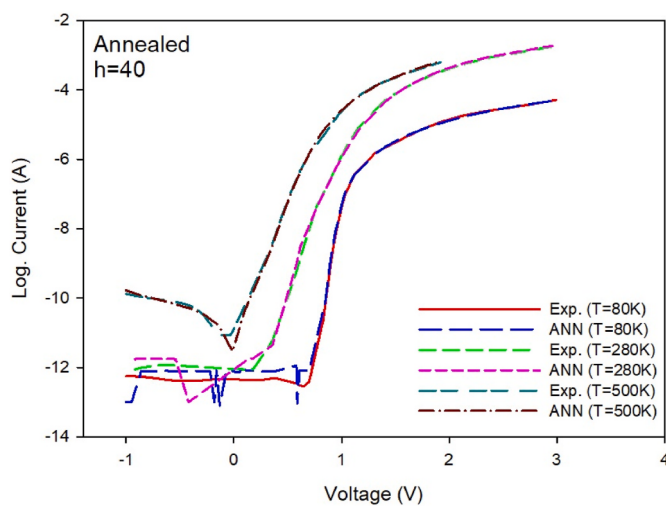


Fig. 4. Experimental and ANN estimated ($H = 40$) current values for annealed test data according to voltage values at different temperatures.

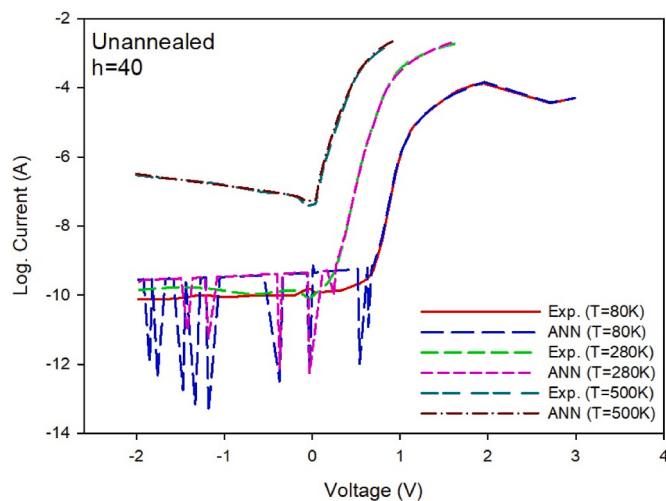


Fig. 5. Experimental and ANN estimated ($H = 40$) current values for unannealed test data according to voltage values at different temperatures.

was obtained in the structure where the number of hidden layer neurons was 5.

Similar results are encountered when the variation of the number of hidden layer neurons on the annealed and un-annealed test data are investigated. When the comparison between the experimental data and the ANN results on the annealed data is examined, it is seen that the RMSE value is high when the number of hidden layer neurons is 5. As the number of hidden neurons increased, this value decreased, and finally, the minimum value was achieved when it reached 40. Then, with the increase in the number of hidden layer neurons, the RMSE value increased again. The RMSE value obtained when the number of hidden layer neurons is 40 is 1.51E-05. The smallest MAE value was obtained as 4.93E-06 when the number of hidden neurons was 40. When the number of hidden neurons is 8, the MAE value is 1.67E-05, the largest.

For un-annealed data, a decrease was observed in the RMSE value with the increase in the number of hidden neurons, and the minimum value was obtained when the number of neurons reached 40. With the increase in the number of hidden neurons again, the RMSE value also increased. The RMSE value obtained when the number of hidden layer neurons is 40 is 5.61E-05. When the MAE values were examined on the un-annealed data, it was observed that the smallest value, 1.30E-05, was

obtained when the number of hidden neurons was 40. The most considerable MAE value was obtained when the number of hidden neurons was five as 3.40E-05.

By examining the error values of the annealed and un-annealed training and test data, it was concluded that the estimation of the Schottky diode characteristics could be made well if the number of hidden neurons is 40. Among these, we decided to present the situation graphs with 30 hidden neurons within the scope of this study. In Fig. 2, the ANN predictions on the annealed data under different temperatures are presented. Cases where the temperature starts from 80 K and reaches 500 K in increments of 20, are given separately. The vertical axes in the graph show the differences in the ANN predictions from the experimental data. When the graphs from 80 K to 340 K are examined, it is seen that the deviations are in the range of -1 V to $+1 \text{ V}$. After the temperature of 360 K, the error range narrowed to the range of -1 V – 0 V . This situation continued until 420 K. After the temperature of 440 K, the deviations stuck around 0 V , and at 500 K showed a small peak at $+1 \text{ V}$. The fact that the difference values in the graphs are observed more on the negative side indicates that the ANN estimates are larger than the experimental values.

In Fig. 3, the deviations of the ANN estimates on the un-annealed data from the experimental data under different temperatures. The results in cases where the temperature starts from 80 K and reaches 500 K in increments of 20 are given separately. The vertical axes in the graph show the differences in the ANN predictions from the experimental data. When the graphs from 80 K to 240 K are examined, it is seen that the deviations are more in the range of -2 V to $+1 \text{ V}$. After the temperature of 260 K, the error range narrowed to the range of -2 V – 0 V . This situation continued until 360 K. The large deviations observed in the range of 0 V to $+1 \text{ V}$ from the temperature of 380 K started to intensify around 0 V after 400 K. The fact that the ANN estimates were larger than the experimental data caused the deviations to be concentrated on the negative y-axis.

Fig. 4 shows the predictions of the ANN structure, in which the number of hidden neurons is 40, on the annealed test data. As can be seen from the graphs drawn separately for different temperature values, the ANN estimates generally agree with the experimental values. Except for the fluctuations in the current at low voltage values (-1 V to $+1 \text{ V}$), it is seen that the ANN estimates are in complete agreement with the experimental data. After the temperature of 440 K, the low voltage values also disappeared in the experimental data. Thus, the ANN estimates fully agreed with the experiment at low voltages for these temperatures.

For un-annealed data, the fluctuations in current are slightly greater at lower voltages. Fig. 5 shows the predictions of the ANN structure with 40 hidden neurons on un-annealed test data for different temperatures. As can be seen from the figure, the ANN estimates are in good agreement with the experimental values. Except for fluctuations in current at low voltage values (-2 V to $+1 \text{ V}$), it is seen that the ANN estimates are in complete agreement with the experimental data up to 360 K. It was observed that the fluctuations in low voltage values disappeared after the temperature of 380 K. The ANN was in complete agreement with the experimental data.

4. Conclusion

In this study, the ANN approach was proposed for modeling the temperature-dependent current-voltage characteristic of fabricated and annealed Ni/n-type 6H-SiC Schottky diode. 7840 samples of experimental data for directly fabricated and 5796 samples of experimental data for annealed diode have been acquired. The data sets have been used to train and test the ANN models with 5-fold cross-validation. The effect of the number of neurons on the modeling performance has been investigated for both modelings of the annealed and non-annealed model in both the training and test phase. The best values for RMSE and MAE have been obtained with 40 neurons in the hidden layer. The

best modeling performance of non-annealed diode characterization has been obtained with 1.55E-05 and 1.51E-05 RMSE values for the training and test phase, respectively. On the other hand, for the annealed diode modeling, the best modeling performance of annealed diode characterization has been obtained with 6.36E-05 and 5.61E-05 RMSE values for the training and test phase, respectively. Although the modeling performance of annealed one is a bit behind that of fabricated, the results show that ANN has a good approximation performance on modeling of I-V characteristic of the Schottky diode within the wide temperature range.

CRediT authorship contribution statement

Hülya Doğan: Writing – original draft, Methodology, Investigation. **Songül Duman:** Investigation, Data curation. **Yunis Torun:** Software, Methodology, Formal analysis. **Serkan Akkoyun:** Validation, Methodology. **Seydi Doğan:** Investigation, Data curation. **Ügur Atıcı:** Writing – review & editing, Visualization.

Declaration of competing interest

The authors declare that they have no known competing financial interests or personal relationships that could have appeared to influence the work reported in this paper.

References

- [1] C. Temirci, M. Gülcen, K. Göksen, M. Sönmez, Ohmic and rectifier properties of Al/Ligand(N-APTH) and Al/Cu(II)Complex contacts, *Microelectron. Eng.* 87 (11) (2010) 2282–2287, <https://doi.org/10.1016/j.mee.2010.03.004>.
- [2] A. Türüt, On current-voltage and capacitance-voltage characteristics of metal-semiconductor contacts, *Turk. J. Phys.* 44 (2021) 302–347, <https://doi.org/10.3906/fiz-2007-11>.
- [3] R.T. Tung, Recent advances in Schottky barrier concepts, *Mater. Sci. Eng. R Rep.* 35 (1) (2001), [https://doi.org/10.1016/S0927-796X\(01\)00037-7](https://doi.org/10.1016/S0927-796X(01)00037-7), 1–138.
- [4] E.H. Rhoderick Williams, Metal-semiconductor Contacts, second ed., Oxford Clarendon, 1988 <https://doi.org/10.1109/ESSDERC.2017.8066606>. R. Rupp, CoolSiC™ and major trends in SiC power device development, in: 2017 47th European Solid-State Device Research Conference (ESSDERC), (2017).
- [5] R. Rupp, CoolSiC™ and major trends in SiC power device development, in: 2017 47th European Solid-State Device Research Conference (ESSDERC), 2017, <https://doi.org/10.1109/ESSDERC.2017.8066606>.
- [6] B. Casady, R.W. Johnson, Status of silicon carbide (SiC) as a wide-bandgap semiconductor for high-temperature applications: a review, *Solid State Electron.* 39 (1996) 1409–1422, [https://doi.org/10.1016/0038-1101\(96\)00045-7](https://doi.org/10.1016/0038-1101(96)00045-7).
- [7] R. Madar, Materials science: silicon carbide in contention, *Nature* (2004) 974–975, <https://doi.org/10.1038/430974a>.
- [8] B.J. Baliga, *Silicon Carbide Power devices*, World Scientific, 2006, pp. 15–33.
- [9] S. Duman, S. Doğan, B. Gürbulak A. Türüt, The barrier-height inhomogeneity in identically prepared Ni/n-type 6H-SiC Schottky diodes, *Appl. Phys.* 91 (2008) 337–340, <https://doi.org/10.1007/s00339-008-4411-8>.
- [10] A. Sefaoğlu, S. Duman, S. Doğan, B. Gürbulak, S. Tüzemen, A. Türüt, The effects of the temperature and annealing on current-voltage characteristics of Ni/n-type 6H-SiC Schottky diode, *Microelectron. Eng.* (2008) 631–635, <https://doi.org/10.1016/J.MEE.2007.11.005>.
- [11] S. Doğan, D. Johnstone, F. Yun, S. Sabuktagin, J. Leach, A.A. Baski, H. Morkoç, The effect of hydrogen etching on 6H-SiC studied by temperature-dependent current-voltage and atomic force microscopy, *Appl. Phys. Lett.* 85 (2004) 1547–1549, <https://doi.org/10.1063/1.1786632>.
- [12] J.R. Nicholls, Electron trapping effects in SiC Schottky diodes: review and comment, *Microelectron. Reliab.* 127 (2021), 114386.
- [13] X. Liao, Y. Liu, J. Li, J. Cheng, Y. Yang, A possible single event burnout hardening technique for SiC Schottky barrier diodes, *Superlattice. Microst.* 160 (2021), 107087, <https://doi.org/10.1016/j.spmi.2021.107087>.
- [14] R. Singh, J.A. Cooper, M.R. Melloch, T.P. Chow, J.W. Palmour, SiC power Schottky and PiN diodes[J], *IEEE Trans. Electron. Dev.* 49 (4) (2002) 665–672, <https://doi.org/10.1109/16.992877>.
- [15] A. Itoh, T. Kimoto, H. Matsunami, High performance of high-voltage 4H-SiC Schottky barrier diodes, *IEEE Electron. Device Lett.* 16 (6) (1995) 280–282, <https://doi.org/10.1109/55.790735>.
- [16] A. Itoh, T. Kimoto, H. Matsunami, Excellent reverse blocking characteristics of high-voltage 4H-SiC Schottky rectifiers with boron-implanted edge termination, *IEEE Electron. Device Lett.* 17 (3) (1996) 139–141, <https://doi.org/10.1109/55.485193>.
- [17] C.E. Weitzel, J.W. Palmour, C.H. Carter, K. Moore, K.J. Nordquist, S. Alien, C. Thero, M. Bhatnagar, Silicon carbide high-power devices, *IEEE Trans. Electron. Dev.* (1993) 43, <https://doi.org/10.1109/16.53681>.
- [18] K. Rottner, M. Frischholz, T. Myrteit, D. Mou, K. Nordgren, A. Henry, C. Hallin, U. Gustafsson, A. Schöner, SiC power devices for high voltage applications, *Mater. Sci. Eng. B* 61–62 (1999) 330–338, [https://doi.org/10.1016/S0921-5107\(98\)00528-5](https://doi.org/10.1016/S0921-5107(98)00528-5).
- [19] K. Järendahl, R.F. Davis, Materials properties and characterization of SiC, in: 52nd ed., in: R. Willardson, E. Weber (Eds.), *Semicond. Semimetals*, Academic Press, New York, NY, 1998, pp. 1–18. <https://www.elsevier.com/books/sic-materials-and-devices/willardson/978-0-12-752160-2>.
- [20] M.E. Levinshtein, S.L. Rumyantsev, M.S. Shur, *Properties of Advanced Semiconductor Materials GaN*, 2001. AlN, InN, BN, SiC, SiGe.
- [21] A. Rabehi, B. Nail, H. Helal, A. Douara, A. Ziane, M. Amrani, B. Akkal, Z. Benamara, Optimal estimation of Schottky diode parameters using a novel optimization algorithm: equilibrium optimizer, *Superlattice. Microst.* 146 (2020), 106665, <https://doi.org/10.1016/j.spmi.2020.106665>.
- [22] W.J. Schaffer, G.H. Negley, K.G. Irvine, JW palmour in diamond, silicon carbide and nitride wide bandgap semiconductors, in: C.H. Carter, G. Gildenbalt, S. Nakamura, R. Nemanich (Eds.), *Mater. Res. Soc. Proc.* vol. 339, 1994, pp. 595–600. Pittsburgh, PA.
- [23] T. Kimoto, H. Nishino, W.S. Yoo, H. Matsunami, Growth mechanism of 6H-SiC in step-controlled epitaxy, *Journal of Applied Physics* 73 (1993) 726–732, <https://doi.org/10.1063/1.353329>.
- [24] V. Kumar, S. Pawar, A.S. Maan, J. Akhtar, Diameter dependent thermal sensitivity variation trend in Ni/4H-SiC Schottky diode temperature sensors, *Vac. Sci. Technol. B, Nanotechnol. Microelectron. Mater. Process. Meas. Phenom.* 33 (2015), 052207, <https://doi.org/10.1116/1.4929890>.
- [25] G. Pristavu, G. Brezeanu, R. Pascu, F. Drăghici, M. Bădilă, Characterization of non-uniform Ni/4H-SiC Schottky diodes for improved responsivity in high-temperature sensing Mater. Sci. Semicond. Process. 94 (2019) 64–69, <https://doi.org/10.1016/j.mssp.2019.01.018>.
- [26] S. Duman, A. Turut, S. Doğan, Thermal sensitivity and barrier height inhomogeneity in thermally annealed and un-annealed Ni/n-6H-SiC Schottky diodes, *Sensors and Actuators: A. Physical* 338 (2022), 113457, <https://doi.org/10.1016/j.sna.2022.113457>.
- [27] F. Roccaforte, F. La Via, A. Baeri, V. Rainieri, L. Calcagno, F. Mangano, Structural and electrical properties of Ni/Ti Schottky contacts on silicon carbide upon thermal annealing, *J. Appl. Phys.* 96 (2004) 4313–4318, <https://doi.org/10.1063/1.1787138>.
- [28] L.M. Porter, R.F. Davis, A critical review of ohmic and rectifying contacts for silicon carbide, *Mater. Sci. Eng. B* 34 (2–3) (1995) 83–105.
- [29] J.N. Su, A.J. Steckl, Fabrication of high voltage SiC Schottky barrier diodes by Ni metallization, 1995, *Silicon Carbide Relat. Mater.* 142 (1996) 697–700.
- [30] K.V. Vassilevski, I.P. Nikitina, N.G. Wright, A.B. Horsfall, A.G. O'Neill, Device processing and characterisation of high temperature silicon carbide Schottky diodes, *Microelectron. Eng.* 83 (1) (2006) 150–154.
- [31] F. La Via, F. Roccaforte, A. Makhtari, V. Rainieri, P. Musumeci, L. Calcagno, Structural and electrical characterisation of nickel silicides contacts on silicon carbide, *Microelectron. Eng.* 60 (2002) 269–282, [https://doi.org/10.1016/S0167-9317\(01\)00604-9](https://doi.org/10.1016/S0167-9317(01)00604-9).
- [32] N. Karaboga, S. Kockanat, H. Dogan, Parameter determination of the Schottky barrier diode using by artificial bee colony algorithm, in: 2011 International Symposium on Innovations in Intelligent Systems and Applications, 2011, <https://doi.org/10.1109/INISTA.2011.594604>.
- [33] A. Rabehi, B. Nail, H. Helal, A. Douara, A. Ziane, M. Amrani, B. Akkal, Z. Benamara, Optimal estimation of Schottky diode parameters using advanced swarm intelligence algorithms, *Semiconductors* 54 (11) (2020) 1398–1405, <https://doi.org/10.1134/S1063782620110214>.
- [34] Y. Torun, H. Doğan, Modeling of Schottky diode characteristic by machine learning techniques based on experimental data with wide temperature range, *Superlattice. Microst.* 160 (2021), 107062, <https://doi.org/10.1016/J.SPMI.2021.107062>.
- [35] A.B. Çolak, T. Güzel, O. Yıldız, M. Özer, An experimental study on determination of the shottky diode current-voltage characteristic depending on temperature with artificial neural network, *Phys. B Condens. Matter* 608 (2021) 412852, <https://doi.org/10.1016/j.physb.2021.412852>.
- [36] S.B. Kutub, H.J. Jiang, N.Y. Chen, W.J. Lee, C.Y. Jui, T.L. Wu, Artificial Neural Network-Based (ANN) Approach for Characteristics Modeling and Prediction in GaN-on-Si Power Devices, 2020 32nd International Symposium on Power Semiconductor Devices and ICs, 2020, <https://doi.org/10.1109/ISPSD46842.2020.9170110>.
- [37] B. Dang, K. Liu, J. Zhu, L. Xu, T. Zhang, C. Cheng, H. Wang, Y. Yang, Y. Hao, R. Huang, Stochastic neuron based on IGZO Schottky diodes for neuromorphic computing, *Appl. Mater. 7* (2019), 071101, <https://doi.org/10.1063/1.5109090>.
- [38] S. Haykin, *N. Network, A comprehensive foundation*, Neural Network. (2004) 241.
- [39] T. Güzel, A.B. Çolak, Artificial intelligence approach on predicting current values of polymer interface Schottky diode based on temperature and voltage: an experimental study, *Superlattice. Microst.* 153 (2021), 106864, <https://doi.org/10.1016/j.spmi.2021.106864>.
- [40] K. Levenberg, A method for the solution of certain non-linear problems in least squares, *Q. Appl. Math.* (1944) 2 164–168, <https://doi.org/10.1090/qam/10666>.
- [41] D.W. Marquardt, An algorithm for least-squares estimation of nonlinear parameters, *J. Soc. Ind. Appl. Math.* 11 (1963) 431–441, <https://doi.org/10.1137/0111030>.